Theory of Magnetic Field-Induced Bose-Einstein Condensation of Triplons in $Ba_3Cr_2O_8$

Tyler Dodds,[1] Bohm-Jung Yang,[1] and Yong Baek Kim[1,2]

[1]*Department of Physics, University of Toronto, Toronto, Ontario M5S 1A7, Canada*
[2]*School of Physics, Korea Institute for Advanced Study, Seoul 130-722, Korea*

(Dated: October 15, 2009)

Motivated by recent experiments on $Ba_3Cr_2O_8$, a new spin-dimer compound with spin-1/2 moments of Cr^{5+} ions, we theoretically investigate the field-induced magnetic ordering in this material in view of the Bose-Einstein condensation (BEC) of triplet excitations (triplons). We apply the self-consistent Hartree-Fock-Popov (HFP) approach to a microscopic Hamiltonian, using the realistic triplon dispersion measured in an inelastic neutron scattering experiment. In particular, we ask to what extent the BEC of dilute triplons near the critical field can explain the magnetic ordering in this material. For example, we investigate the temperature range where the BEC picture of triplons can be applied via the HFP approach. We also determine the temperature regime where a quadratic approximation of the triplon dispersion works. It is found that the strength of the effective repulsive interaction between triplons is much weaker in $Ba_3Cr_2O_8$ than in the canonical spin-dimer compound $TlCuCl_3$. Small effective repulsive interaction in combination with the narrow band of triplons leads to higher density of triplons $n_{\rm cr}$ at the critical point. It turns out that the combined effect points to a bigger HFP correction $Un_{\rm cr}$ in $Ba_3Cr_2O_8$ than in $TlCuCl_3$. Nonetheless, the HFP approach provides a reasonable explanation of the transverse magnetization and the specific heat data of $Ba_3Cr_2O_8$.

PACS numbers: 74.20.Mn, 74.25.Dw

I. INTRODUCTION

Magnetic-field-induced quantum phase transitions in spin dimer systems have provided excellent playgrounds for the investigation of novel universality classes of zero temperature quantum phase transitions.[1] These systems possess non-magnetic spin singlet ground states with a spin gap to triplet excitations (triplons). When a magnetic field H is applied, a quantum phase transition occurs at a critical field H_c, where the spin gap closes and the lowest triplet excitation condenses. At $H > H_c$, the average triplon density is finite and can be controlled by the applied magnetic field.

The resulting ground states are determined by a delicate balance between the kinetic energy and the repulsive interaction between triplons.[2] On one hand, if the triplon hopping processes are suppressed by frustration or the repulsive interaction dominates, the condensed triplons may form a superlattice with broken translational symmetry, leading to magnetization plateaus. This is known to occur, for instance, in $SrCu_2(BO_3)$.[3,4] On the other hand, if the magnetic interaction does not have much frustration or the kinetic energy dominates, the ground state can be described as a Bose-Einstein condensate (BEC) of triplons and form a homogeneous magnetically ordered state. In this case, the magnetically ordered state at $H > H_c$ supports a staggered magnetization transverse to the field direction, leading to a canted antiferromagnetic state (until the system eventually becomes fully polarized as H increases). This type of behavior has been observed, for example, in three-dimensionally coupled spin dimer systems $TlCuCl_3$[5,6] and $BaCuSi_2O_6$,[7] which exhibits unconventional critical behavior.[8–11] Furthermore, recent discoveries of $A_3M_2O_8$,[12] where A = Ba or Sr, and M = Cr or Mn, have provided a lot of excitement for spin dimer system research, as these systems may represent a variety of different spin dimer interactions and quantum ground states.

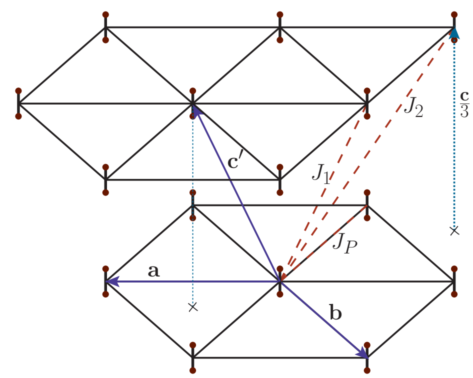

FIG. 1: (colour online) Schematic diagram showing two neighboring triangular lattice planes of dimers in $Ba_3Cr_2O_8$. Two primitive lattice vectors $\mathbf{a}$ and $\mathbf{b}$ are shown in the lower plane. The third primitive lattice vector $\mathbf{c}'$ connects central dimers in the neighboring planes. We set the vertical distance between neighboring planes by $\mathbf{c}$/3. Here we use J_P to indicate the inplane nearest-neighbour interdimer coupling. J_1 (J_2) denotes the nearest-neighbour (next nearest-neighbor) inter-plane dimer coupling.

In this work, we present a theory of the magnetic field-induced quantum phase transition discovered in $Ba_3Cr_2O_8$, where Cr^{5+} carries an S=1/2 moment ($3d^1$).[13] Low temperature bulk susceptibility shows that this compound does not have any magnetic long-range order down to 1.5 K in the absense of an external magnetic field.[14,15] When the external magentic field H reaches $H_{c1} \sim 12$ T, a field-induced transition to a magnetically ordered state occurs and a fully polarized state arises at $H > H_{c2} \sim 23$ T.[13] In this compound, two neighboring S=1/2 Cr^{5+} ions lying along the $\mathbf{c}$ direction form a singlet dimer. In the ab-plane, these dimer singlets are coupled into triangular lattices, which are stacked along the $\mathbf{c}$ direction (see Fig.1). According to recent elastic and inelastic neutron scattering measurements,[12] $Ba_3Cr_2O_8$ is an excellent model system for weakly coupled S =1/2

quantum spin dimers, featuring strong intradimer coupling of J_0=2.38(2) meV and weak interdimer couplings less than 0.52(2) meV.[12] Because of the orbital degeneracy of the Cr^{5+} ion, there is a structural transition around 70 K via a Jahn-Teller distortion, relieving the frustration. As a consequence, spatially anisotropic interdimer couplings arise. The relative orientations of the anisotropic interdimer couplings are described in Fig.2. It was confirmed that the magnetically ordered state has a commensurate and collinear transverse spin component for $H_{c1} < H < H_{c2}$.[13] This is in contrast to the case of $Ba_3Mn_2O_8$ with orbitally non-degenerate S=1 Mn^{5+} ions ($3d^2$), where the geometric frustration and single-ion anisotropy lead to incommensurate spiral order upon triplon condensation.[17]

We first consider the Heisenberg spin Hamiltonian using the spin exchange couplings determined by inelastic neutron scattering measurements.[12] Applying the bond operator formalism, we obtain the dispersion of the lowest energy triplet excitations.[18,19] We confirm that the Hamiltonian written in terms of bond operators at the quadratic level, neglecting singlet fluctuation, leads to the same triplon dispersion as determined in experiment in Ref.12.

We then use the Hartree-Fock-Popov (HFP) approximation combined with the realistic triplon dispersion to interpret two different experimental data sets, those of M. Kofu *et al.* in Ref.13 and A. A. Aczel *et al.* in Ref.16. In particular, we would like to understand to what extent $Ba_3Cr_2O_8$ is a good candidate for the BEC of triplons in comparison to other three-dimensionally coupled spin-dimer systems such as $TlCuCl_3$.[20–22] Within the HFP analysis, we determine the effective inter-triplet repulsion U and the zero-field spin gap Δ in $Ba_3Cr_2O_8$. It turns out that the strength of the effective repulsive interaction U between triplons in $Ba_3Cr_2O_8$ is an order of magnitude smaller than that of $TlCuCl_3$,[21] and smaller than the bandwidth of the triplons as well. This suggests that the system is indeed in the regime where the kinetic energy dominates. In addition, the shape of the dispersion near the triplon band minimum results in the large effective mass of triplons in $Ba_3Cr_2O_8$. As a result, the relation $[H_c(T) - H_c(0)] \propto T^{3/2}$ in three dimensions for quadratic triplon dispersion works only at $T < 0.1$ K, while it works at $T < 1$ K in $TlCuCl_3$. The HFP approach is used to describe other experimental measurements such as the longitudinal and transverse staggered magnetizations and the heat capacity. Despite the simplicity of the theoretical approach, the HFP approximation is found to explain these physical properties even quantitatively.

The rest of the paper is organized as follows. In Sec.II we use the bond operator approach to obtain the triplet dispersion from the microscopic Hamiltonian. Theoretical description of the triplon Bose-Einstein condensation within the HFP approximation is discussed in detail in Sec.III. In Sec.IV, we apply the HFP approach to explain the experimental data and draw the phase diagram in the plane of H_c versus T. The HFP approach is applied to describe the heat capacity in Sec.V and the magnetization measurements in Sec.VI. Finally, in Sec.VII, we summarize our result, and discuss possible limitations and extensions of the current work.

II. TRIPLON DISPERSION VIA BOND-OPERATOR APPROACH

Since the intradimer exchange interaction dominates all the other interdimer couplings in $Ba_3Cr_2O_8$, it is natural to take advantage of the bond-operator representation of the singlet and triplet dimer states.[23,24] This is achieved by placing one singlet or triplet boson on each dimer, to represent the states

$$\begin{aligned}
|s\rangle &= s^\dagger |0\rangle = \frac{|\uparrow\downarrow\rangle - |\downarrow\uparrow\rangle}{\sqrt{2}}, \\
|t_0\rangle &= t_0^\dagger |0\rangle = \frac{|\uparrow\downarrow\rangle + |\downarrow\uparrow\rangle}{\sqrt{2}}, \\
|t_+\rangle &= t_+^\dagger |0\rangle = -|\uparrow\uparrow\rangle, \\
|t_-\rangle &= t_-^\dagger |0\rangle = |\downarrow\downarrow\rangle,
\end{aligned} \tag{1}$$

where the quantization z-axis is taken to be the applied field direction. The triplet states $|t_m\rangle$ ($m = 1, 0, -1$) are chosen as the S_z eigenstates satisfying $S_z|t_m\rangle = m\hbar|t_m\rangle$. The hard-core constraint $s^\dagger s + t_0^\dagger t_0 + t_+^\dagger t_+ + t_-^\dagger t_- = 1$ is enforced on each dimer, ensuring that the physical state is exactly one of the four above.

The two spin operators constituting a dimer can be rewritten in terms of the bosonic bond operators as

$$\begin{aligned}
S_{1\alpha} &= \frac{1}{2}\left(s^\dagger t_\alpha + t_\alpha^\dagger s - i\epsilon_{\alpha\beta\gamma} t_\beta^\dagger t_\gamma\right), \\
S_{2\alpha} &= \frac{1}{2}\left(-s^\dagger t_\alpha - t_\alpha^\dagger s - i\epsilon_{\alpha\beta\gamma} t_\beta^\dagger t_\gamma\right)
\end{aligned} \tag{2}$$

with $\alpha \in \{x, y, z\}$ and ϵ the totally antisymmetric tensor. This form gives the correct matrix elements in the singlet-triplet Hilbert space. We define $|t_\alpha\rangle$ triplons as eigenstates with $S_\alpha |t_\alpha\rangle = 0$ so that $t_z = t_0$, $t_x = \frac{1}{\sqrt{2}}(t_- + t_+)$ and $t_y = \frac{i}{\sqrt{2}}(t_- - t_+)$. We henceforth assume a sum over repeated indices.

Besides connecting spin operators to singlet and triplet boson operators, the bond operator formalism naturally yields a triplon dispersion from the microscopic Hamiltonian. We consider a Heisenberg spin Hamiltonian with intra-dimer coupling, and coupling between nearby dimers. We include nearest neighbor interactions between dimers on the same plane. Between adjacent planes, we include interactions between first and second-nearest neighboring dimers. The tetrahedrally-coordinated $3d^1$ electron in Cr^{5+} has e_g orbital degeneracy and undergoes Jahn-Teller distortion. This gives rise to spatially anisotropic interdimer interactions.[12] The in-plane projection of the anisotropic interdimer interactions are described in Fig.2.

The intra-dimer coupling has a strength of $J_0 = 2.38$ meV. Table I displays the values and directions of the couplings to nearby dimers depicted in detail in Fig.2. These strengths have been determined in Ref.12 by fitting an RPA dispersion to the triplon dispersion measured by inelastic neutron scattering.

There are four possible spin-spin interactions between two dimers at sites i and j. However, at quadratic order in the t

m	J_m (meV)	$\Delta\mathbf{r}_m$
1	$J'_P = 0.1$	$\mathbf{a}$
2	$J''_P = 0.07$	$\mathbf{b}$
3	$J'''_P = -0.52$	$-\mathbf{a}-\mathbf{b}$
4	$J'_1 = 0.08$	$2\mathbf{a}/3+\mathbf{b}/3+\mathbf{c}/3$
5	$J''_1 = -0.15$	$-\mathbf{a}/3+\mathbf{b}/3+\mathbf{c}/3$
6	$J'''_1 = 0.1$	$-\mathbf{a}/3-2\mathbf{b}/3+\mathbf{c}/3$
7	$J'_2 = 0.04$	$-4\mathbf{a}/3-2\mathbf{b}/3+\mathbf{c}/3$
8	$J''_2 = 0.1$	$2\mathbf{a}/3-2\mathbf{b}/3+\mathbf{c}/3$
9	$J'''_2 = 0.09$	$2\mathbf{a}/3+4\mathbf{b}/3+\mathbf{c}/3$

TABLE I: Interaction strength J_m and relative distance $\Delta\mathbf{r}_m$ for the nine different anisotropic interdimer couplings as described in Fig.2.

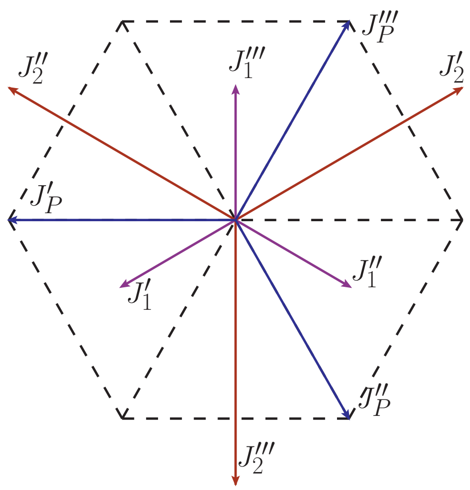

FIG. 2: (colour online) In-plane projection of the strengths and directions of the different anisotropic interdimer couplings considered in this work. The couplings J_P are in-plane nearest neighbor couplings, which are represented by dashed lines. J_1 (J_2) is the first (second) nearest-neighbour interplane coupling.

bosons, $\mathbf{S}_{i1}\cdot\mathbf{S}_{j1} = \mathbf{S}_{i2}\cdot\mathbf{S}_{j2} = -\mathbf{S}_{i1}\cdot\mathbf{S}_{j2} = -\mathbf{S}_{i2}\cdot\mathbf{S}_{j1}$. All of the potential spin-spin Heisenberg interactions between two dimers thus reduce to a single effective interaction J_m. With this, we take the Hamiltonian to be

$$\mathcal{H} = \sum_i J_0 \mathbf{S}_{i1}\cdot\mathbf{S}_{i2} + \sum_i \sum_{m=1}^{9} J_m \mathbf{S}_{i,1}\cdot\mathbf{S}_{i+\delta\mathbf{r}_m,1}, \quad (3)$$

where the intra-dimer interaction can be written as

$$J_0\mathbf{S}_{1i}\cdot\mathbf{S}_{2i} = J_0\left(-\frac{3}{4}s_i^\dagger s_i + \frac{1}{4}t_{i\alpha}^\dagger t_{i\alpha}\right). \quad (4)$$

We now investigate the ground state and the excitations of this Hamiltonian in the low temperature regime where the intra-dimer interaction dominates. Singlets are energetically favourable in this case, with macroscopic occupation, we can take them to be condensed. This process ignores singlet fluctuations by replacing the spin operators $s_i^\dagger$ and s_i with a complex number $\bar{s}$, creating a uniform condensate.

Condensing the singlets leaves a Hamiltonian describing the triplets. Inter-dimer interactions lead to triplon excitation dispersion in momentum space. Our analysis considers the low triplon density limit, so we retain terms up to quadratic order in the t operators. To impose the hardcore constraint we introduce a site-dependent chemical potential μ_i. This adds to the Hamiltonian the constraint term

$$\sum_i \mu_i\left(1 - s_i^\dagger s_i - t_{i\alpha}^\dagger t_{i\alpha}\right). \quad (5)$$

To make a tractible analysis, the above constraint is enforced in a mean-field manner taking $\mu_i = \mu$, on average over the entire lattice. In the momentum representation, this gives $\bar{s}^2 + \int\frac{\mathrm{d}^3k}{(2\pi)^3} t_{\mathbf{k}\alpha}^\dagger t_{\mathbf{k}\alpha} = 1$. At $T=0$, the values of μ and $\bar{s}$ are determined from the saddle point condition. First, $\left\langle\frac{\partial\mathcal{H}}{\partial\mu}\right\rangle = 0$ enforces the constraint $0 = \sum_i\left(1 - \left\langle s_i^\dagger s_i\right\rangle - \left\langle t_{i\alpha}^\dagger t_{i\alpha}\right\rangle\right)$, as expected. Second, the condition $\left\langle\frac{\partial\mathcal{H}}{\partial\bar{s}}\right\rangle = 0$ minimizes the ground-state energy with respect to the singlet density.

Our Hamiltonian obtains a quadratic form in the momentum space: $\mathcal{H} = N_d\epsilon_0 + \mathcal{H}_0 + \mathcal{H}_\pm$. Here N_d denotes the number of dimers on the lattice. The t_0 triplons interact with themselves but not the other triplon species. They contribute with the quadratic Hamiltonian

$$\mathcal{H}_0 = \frac{1}{2}\sum_{\mathbf{k}}\left(t_{\mathbf{k}0}^\dagger \;\; t_{-\mathbf{k}0}\right)\begin{pmatrix} A_\mathbf{k} & B_\mathbf{k} \\ B_\mathbf{k}^* & A_\mathbf{k}^*\end{pmatrix}\begin{pmatrix} t_{\mathbf{k}0} \\ t_{-\mathbf{k}0}^\dagger\end{pmatrix}, \quad (6)$$

where $A_\mathbf{k} = \frac{J_0}{4} - \mu + B_\mathbf{k}$, with

$$B_\mathbf{k} = -\bar{s}^2\sum_m J_m\cos\left(\mathbf{k}\cdot\Delta\mathbf{r}_m\right). \quad (7)$$

$\mathcal{H}_0$ can be diagonalized by the Bogolibov transormation $\gamma_{\mathbf{k}0} = u_\mathbf{k} t_{\mathbf{k}0} + v_\mathbf{k} t_{-\mathbf{k}0}^\dagger$, with quasiparticle energy[25]

$$\omega_\mathbf{k} = \sqrt{A_\mathbf{k}^2 - B_\mathbf{k}^2} = \sqrt{(\frac{J_0}{4}-\mu)^2 + 2(\frac{J_0}{4}-\mu)B_\mathbf{k}}. \quad (8)$$

Neither t_0 nor γ_0 are subject to Zeeman splitting by the external field. However, the t_+ and t_- triplons are split. Furthermore, they interact with each other. The resultant quadratic Hamiltonian $\mathcal{H}_\pm$ is

$$\mathcal{H}_\pm = \frac{1}{2}\sum_\mathbf{k}\Psi_\mathbf{k}^\dagger\begin{pmatrix} A_\mathbf{k}-h & 0 & 0 & B_\mathbf{k} \\ 0 & A_\mathbf{k}+h & B_\mathbf{k} & 0 \\ 0 & B_\mathbf{k} & A_\mathbf{k}-h & 0 \\ B_\mathbf{k} & 0 & 0 & A_\mathbf{k}+h\end{pmatrix}\Psi_\mathbf{k}, \quad (9)$$

where $h = g\mu_B H$ and $\Psi_\mathbf{k}^\dagger$=($t_{\mathbf{k}+}^\dagger$ $t_{\mathbf{k}-}^\dagger$ $t_{-\mathbf{k}+}$ $t_{-\mathbf{k}-}$). $\mathcal{H}_\pm$ is diagonalized into quasiparticles $\gamma_{\mathbf{k}\pm}$ with energy $\omega_\mathbf{k}\mp h$, where

$$\begin{aligned}\gamma_{\mathbf{k}+}^\dagger &= u_{\mathbf{k}+}t_{\mathbf{k}+}^\dagger + v_{\mathbf{k}+}t_{-\mathbf{k}-}, \\ \gamma_{\mathbf{k}-}^\dagger &= u_{\mathbf{k}-}t_{\mathbf{k}-}^\dagger + v_{\mathbf{k}-}t_{-\mathbf{k}+},\end{aligned} \quad (10)$$

$$\begin{aligned} u_{\mathbf{k}+} &= \frac{B_\mathbf{k}}{\sqrt{2\omega_\mathbf{k}(A_\mathbf{k}-\omega_\mathbf{k})}},\; v_{\mathbf{k}+} = \frac{A_\mathbf{k}-\omega_\mathbf{k}}{\sqrt{2\omega_\mathbf{k}(A_\mathbf{k}-\omega_\mathbf{k})}}, \\ u_{\mathbf{k}-} &= \frac{A_\mathbf{k}+\omega_\mathbf{k}}{\sqrt{2\omega_\mathbf{k}(A_\mathbf{k}+\omega_\mathbf{k})}},\; v_{\mathbf{k}-} = \frac{B_\mathbf{k}}{\sqrt{2\omega_\mathbf{k}(A_\mathbf{k}+\omega_\mathbf{k})}}. \end{aligned} \quad (11)$$

The γ_+ triplon, with spin along the quantization axis, will be the focus of the HFP treatment, since it interacts with no other species and lowers its energy from the Zeeman splitting. Finally, the constant part of the Hamiltonian is given by

$$\epsilon_0 = -\frac{3}{4}J_0\bar{s}^2 + \mu(1-\bar{s}^2) - \frac{3}{2N_d}\sum_{\mathbf{k}} A_{\mathbf{k}}. \quad (12)$$

In the limit of vanishing inter-dimer interactions (in this case, all $J', J'', J''' \to 0$), the saddle-point solution gives $\bar{s} = 1$ and $\mu = -\frac{3}{4}J_0$. This limit serves as a good starting point in $Ba_3Cr_2O_8$, where J_0 is much larger than the inter-dimer couplings. Furthermore, with these values of $\bar{s}$ and μ, the triplon dispersion matches the RPA form fitted to experimental values in Ref.12. Solving the saddle-point conditions with the couplings in Table I taken as bare values, we find $\bar{s} = 0.992$ and $\mu = -0.775J_0$, showing a high degree of dimerization. The bare couplings will be slightly renormalized (compared to the $\bar{s} = 1$, $\mu = -3J_0/4$ case) as a result. In particular, $J_0 \to J_0 - \Delta\mu$ and $J_m \to \bar{s}^2 J_m$ for $m \in \{1, \ldots, 9\}$. However, we can take these renormalized couplings to have the values in Table I, since only the final dispersion will be used in our Hartree-Fock calculation. We furthermore assume that the dispersion is not temperature dependent within the low-temperature regime considered.

III. HARTREE-FOCK EFFECTIVE HAMILTONIAN

We turn our focus to the γ_+ quasiparticle; being the field-aligned quasiparticle, it will condense with sufficiently large Zeeman splitting. We consider field strengths large enough that we may ignore the higher-energy γ_0 and γ_- quasiparticles. The typical splitting is of energy $g\mu_b H_c(0) \cong 15.4$ K. This scale is significantly larger than the highest temperature (around 2.7 K) where the BEC transition occurs[16]. Consequently, ignoring terms in the Hamiltonian with γ_0 and γ_- is a safe approximation to make in this external field regime.

The Hamiltonian we take for the $b \equiv \gamma_+$ triplons is $\mathcal{H} = \mathcal{H}_K + \mathcal{H}_U$, which is the sum of the kinetic and inter-triplon interaction terms. Here,

$$\mathcal{H}_K = \sum_{\mathbf{k}} (\epsilon_k - \mu)\, b^\dagger_{\mathbf{k}} b_{\mathbf{k}}, \quad (13)$$

$$\mathcal{H}_U = \frac{1}{2N_d}\sum_{\mathbf{k},\mathbf{k}',\mathbf{q}} U_{\mathbf{q}} b^\dagger_{\mathbf{k}} b^\dagger_{\mathbf{k}'} b_{\mathbf{k}+\mathbf{q}} b_{\mathbf{k}'-\mathbf{q}}, \quad (14)$$

where $\mu = g\mu_B H - \Delta$ is the chemical potential and Δ is the zero-field gap (1.37 meV from the bond-operator theory). $\epsilon_{\mathbf{k}} + \Delta$ is the zero-field dispersion with $\epsilon_{\mathbf{k}}$ determined from the bond-operator theory. The quartic terms from the bond-operator theory give rise to interactions between the b triplons. Combined with the interaction from the hard-core constraint, this gives an approximate form for $U_{\mathbf{q}}$. However, in the low-temperature limit where the excited triplons lie near the band minimum at $\mathbf{Q}$, we may approximate $U_{\mathbf{q}} \approx U_{\mathbf{Q}}$ as a constant, U. The value of the interaction parameter U will be determined from a fit to the experimental data.

The condensate will form at the dispersion minimum $\mathbf{Q} = \frac{1}{2}(\mathbf{u}+\mathbf{v})$[13]. Note that we define the reciprocal lattice vectors $\mathbf{u}$, $\mathbf{v}$, and $\mathbf{w}$ in the conventional way. For example, $\mathbf{u} = 2\pi\frac{\mathbf{b}\times\mathbf{c}}{\mathbf{a}\cdot(\mathbf{b}\times\mathbf{c})}$. We follow the Hartree-Fock-Popov approach of Ref. 21 by condensing the triplons at $\mathbf{Q}$: $b^\dagger_{\mathbf{Q}},\ b_{\mathbf{Q}} \to \sqrt{N_d n_c}$, where n_c is the condensate density (the condensed boson fraction per dimer). Introducing the summation $\sum'$, which excludes any terms containing creation or annihilation operators at momentum $\mathbf{k} = \mathbf{Q}$, we decompose $\mathcal{H}_U$ as follows:

$$\begin{aligned}\mathcal{H}_U = &\frac{U}{2N_d}N_c^2 + \frac{UN_c}{N_d}\sum_{\mathbf{q}}{}' \left\{\frac{b_{\mathbf{q}}b_{-\mathbf{q}} + b^\dagger_{-\mathbf{q}}b^\dagger_{\mathbf{q}}}{2} + 2b^\dagger_{\mathbf{q}}b_{\mathbf{q}}\right\}\\ &+ \frac{U\sqrt{N_c}}{N_d}\sum_{\mathbf{k},\mathbf{q}}{}' \left\{b^\dagger_{\mathbf{k}}b_{\mathbf{k}+\mathbf{q}}b_{\mathbf{Q}-\mathbf{q}} + h.c.\right\}\\ &+ \frac{U}{2N_d}\sum_{\mathbf{k},\mathbf{k}',\mathbf{q}}{}' b^\dagger_{\mathbf{k}}b^\dagger_{\mathbf{k}'}b_{\mathbf{k}+\mathbf{q}}b_{\mathbf{k}'-\mathbf{q}}, \end{aligned} \quad (15)$$

using the fact that $2\mathbf{Q}$ is a reciprocal lattice vector, so that $b_{-\mathbf{k}+\mathbf{Q}} = b_{-(\mathbf{k}+\mathbf{Q})}$. Performing a mean-field quadratic decoupling of the quartic terms yields the following mean-field quadratic Hamiltonian:

$$\mathcal{H}_{\text{MF}} = E_0 + \sum_{\mathbf{k}}{}' \tilde{\epsilon}_{\mathbf{k}} b^\dagger_{\mathbf{k}} b_{\mathbf{k}} + \frac{Un_c}{2}\sum_{\mathbf{q}}{}' \{b_{\mathbf{q}}b_{-\mathbf{q}} + b^\dagger_{-\mathbf{q}}b^\dagger_{\mathbf{q}}\}, \quad (16)$$

where

$$\begin{aligned} E_0 &= -\mu n_c + UN_d\left(\frac{n_c^2}{2} - (n-n_c)^2\right),\\ \tilde{\epsilon}_{\mathbf{k}} &= \epsilon_{\mathbf{k}} - \tilde{\mu},\\ \tilde{\mu} &= g\mu_B H - \Delta - 2Un. \end{aligned} \quad (17)$$

This decoupling is valid so long as the triplon densities $\left\langle b^\dagger_{\mathbf{k}} b_{\mathbf{k}}\right\rangle$ are small. In the noncondensed (normal) phase, the Hamiltonian is already diagonalized. The triplon density is given by the Bose distribution function, and must be determined self-consistently:

$$n = \int \frac{\mathrm{d}^3k}{(2\pi)^3} f_B(\tilde{\epsilon}_{\mathbf{k}}). \quad (18)$$

In the condensed phase, we must perform another Bogoliubov transformation, which leads to the following diagonalized Hamiltonian:

$$\mathcal{H}_{\text{MF}} = \sum_{\mathbf{k}}{}' E_{\mathbf{k}}\left(\varphi^\dagger_{\mathbf{k}}\varphi_{\mathbf{k}}\right) - \frac{1}{2}\sum_{\mathbf{k}}{}' \tilde{\epsilon}_{\mathbf{k}} + E_0, \quad (19)$$

where

$$\begin{aligned} E_{\mathbf{k}} &= \sqrt{\tilde{\epsilon}^2_{\mathbf{k}} - (Un_c)^2},\\ \varphi_{\mathbf{k}} &= \tilde{u}_{\mathbf{k}} b_{\mathbf{k}} + \tilde{v}_{\mathbf{k}} b^\dagger_{-\mathbf{k}}, \end{aligned} \quad (20)$$

in which

$$\tilde{u}_{\mathbf{k}} = \sqrt{\frac{\tilde{\epsilon}_{\mathbf{k}}}{2E_{\mathbf{k}}} + \frac{1}{2}}, \quad \tilde{v}_{\mathbf{k}} = \sqrt{\frac{\tilde{\epsilon}_{\mathbf{k}}}{2E_{\mathbf{k}}} - \frac{1}{2}}. \quad (21)$$

The number of thermally excited triplons is

$$n - n_c = \int \frac{\mathrm{d}^3k}{(2\pi)^3}\left[\frac{\tilde{\epsilon}_{\mathbf{k}}}{E_{\mathbf{k}}}\left(f_B(E_{\mathbf{k}}) + \frac{1}{2}\right)\right] - \frac{1}{2}. \qquad (22)$$

For the final φ quasiparticles to be condensed at $\mathbf{Q}$, they must be gapless. This constrains the effective chemical potential as $\tilde{\mu} = -Un_c$, so that the field in the condensed phase is given by

$$g\mu_B H = \Delta + U\left(2n - n_c\right). \qquad (23)$$

Between these two phases is the transition curve $H_c(T)$ where triplons begin to condense. The b triplons are gapped in the noncondensed phase. However, at the transition point to the condensed phase, they become gapless. This constrains the effective chemical potential as $\tilde{\mu} = 0$ to give the critical field

$$H_c(T) = \frac{\Delta}{g\mu_B} + \frac{2U}{g\mu_B} n_{\text{cr}}(T). \qquad (24)$$

Since $\tilde{\epsilon}_{\mathbf{k}} = \epsilon_{\mathbf{k}}$ in this case, we determine the critical boson density at the transition, n_{cr}, by the integral

$$n_{\text{cr}} = \int \frac{\mathrm{d}^3k}{(2\pi)^3} f_B(\epsilon_{\mathbf{k}}). \qquad (25)$$

IV. CRITICAL DENSITY PHASE DIAGRAM

In the HFP approach the critical field H_c depends on the critical boson density n_{cr} linearly as shown in Eq.(24). A linear fit of H_c to n_{cr} determines the interaction parameter U from the slope. In addition the zero-temperature critical field $H_c(0)$ gives another estimate for the gap Δ. With a given experimental data (H_c, T), we obtain (H_c,n_{cr}) pairs making use of the Eq.(25). In the low-temperature, low-density regime where HFP approach is valid, we expect H_c to be linear in n_{cr}.

We present three different fits of H_c to n_{cr}. These are based on the two different experimental data sets obtained from Ref.13 and Ref.16. Lines of best fit neglect the high-temperature (density) regimes where H_c loses linearity in n_{cr}. A linear relation between H_c and n_{cr} is achieved for the case of H parallel to the c-axis, as shown in Fig.3 and Fig.4. In Fig.3 we describe the result of the linear fit which is obtained using the experimental data from M. Kofu *et al.* in Ref.13. From the linear relation, we estimate the interaction constant $U \cong 6.5$ K and zero-field spin gap $\Delta \cong 1.35$ meV. The same analysis is performed using the second experimental data set given by A. A. Aczel *et al.* in Ref.16 and the result is shown in Fig.4. This fit gives an estimate of $U \approx 8.7$ K and $\Delta \cong 1.34$ meV, which is very close to the value obtained from the bond-operator approach. Since this experimental data shows smaller deviations from the linear fit, over a larger range of temperatures, we use the estimate of $U \approx 8.7$ K and $\Delta \cong 1.34$ meV in the following analysis. In Fig.5 we display the low temperature phase diagram $H_c(T)$, which is again obtained using the data of Ref.16.

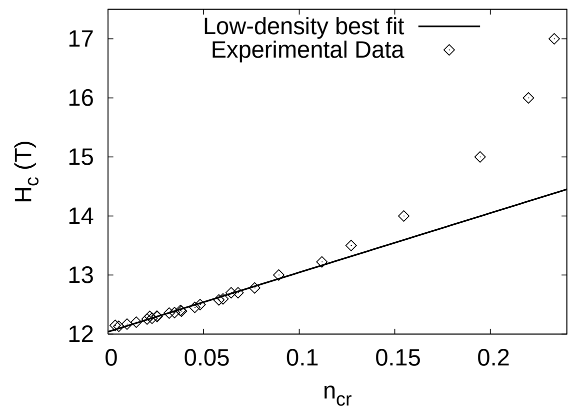

FIG. 3: The critical field H_c as a function of critical density n_{cr} with the applied field H parallel to the c-axis. $n_{\text{cr}}(T)$ is calculated, using the HFP approach, from the given experimental temperatures. A linear fit of H_c to n_{cr} is performed in a low-density range. The experimental data is from M. Kofu *et al.* in Ref.13

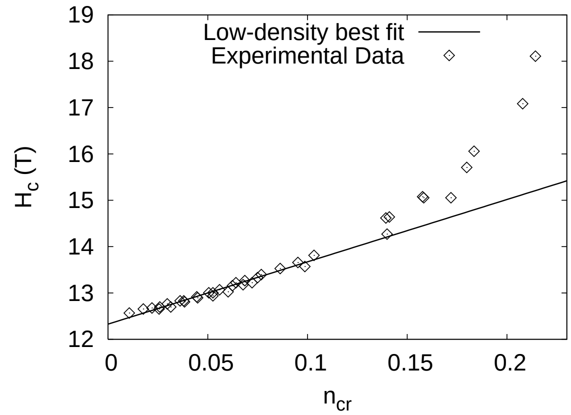

FIG. 4: Same plot as in Fig.3, but the data is from A. A. Aczel *et al.* in Ref.16.

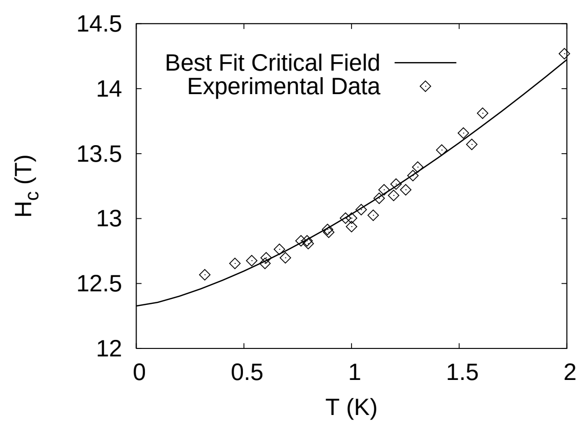

FIG. 5: Phase diagram giving the critical field H_c as a function of temperature. Experimental data is from A. A. Aczel *et al.* in Ref.16, with applied field H parallel to the c-axis. The solid line shows the theoretical result obtained from the HFP approach using the linear fit displayed in Fig.4.

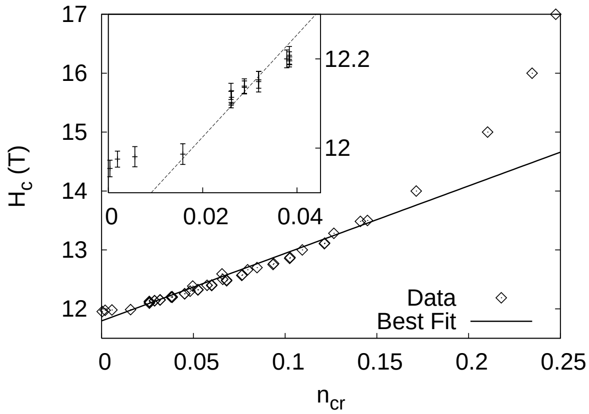

FIG. 6: The critical field H_c (circles) as a function of critical density $n_{\rm cr}$ with the applied field H perpendicular to the c-axis. Here we use the data in Ref.13 . Inset: discrepancy between experiment and the best-fit line in the small $n_{\rm cr}$ regime.

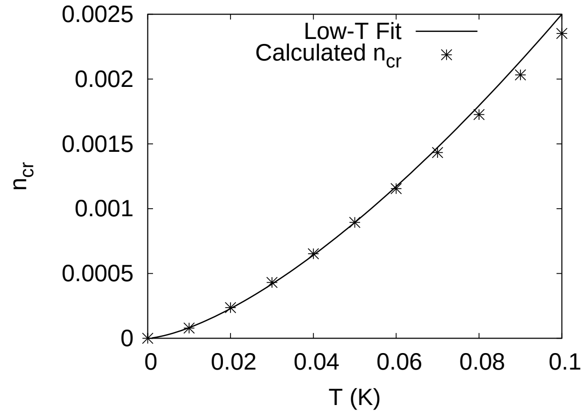

FIG. 8: Critical density $n_{\rm cr}$ of $Ba_3Cr_2O_8$ calculated from the HFP theory with the full dispersion (cross points). The solid line is $T^{\frac{3}{2}}$ power-law fit coming from the simple quadratic dispersion. The points obtained from the full dispersion begin to deviate from the power-law fit around 0.06 K.

On the other hand, the data for H perpendicular to the c-axis features low-temperature behaviour inconsistent with the general linear trend as shown in Fig.6 and its inset. We think that the existence of DM interaction is one possible explanation of this low-temperature discrepancy from the linear behavior. Further discussion on this direction is shown in Sec.VII.

Since a full-dispersion treatment successfully reproduces the phase diagram for the dimerized spin system $TlCuCl_3$,[21] it is instructive to use it in comparison with the HFP approach for $Ba_3Cr_2O_8$. Triplons in $Ba_3Cr_2O_8$ have a smaller self-interaction constant, of $U \approx 8.7$ K, compared to $TlCuCl_3$, which has $U \approx 320$ K.[21] However, triplon densities are significantly higher in $Ba_3Cr_2O_8$ than in $TlCuCl_3$, by over an order of magnitude. This makes the Hartree-Fock critical field shift $Un_{\rm cr}$ greater in $Ba_3Cr_2O_8$ than in $TlCuCl_3$. In Fig.7 we plot $Un_{\rm cr}$ in these two systems with varying temperature. Within

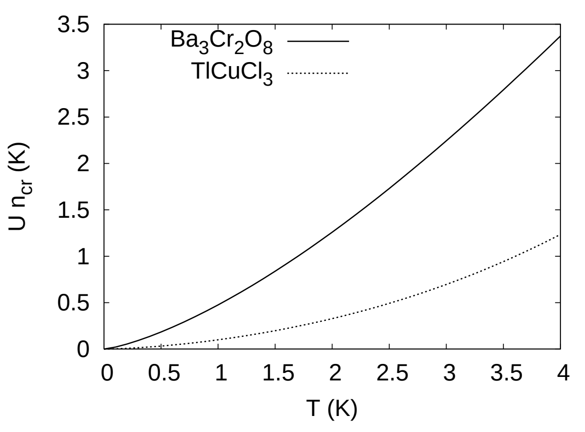

FIG. 7: Comparison of overall interaction energy scale $Un_{\rm cr}$ as a function of temperature between $Ba_3Cr_2O_8$ (solid line) and $TlCuCl_3$ (dashed line) systems. $n_{\rm cr}$ is the density of triplons at the condensate transition and U the inter-triplon interaction strength.

the Hartree-Fock-Popov approach, the term $-2Un$ acts as a shift in the effective chemical potential as shown in Eq.(17). A decrease in U will increase the effective chemical potential, causing an increase in the triplon density as seen with $Ba_3Cr_2O_8$.

The shape of the dispersion affects the temperature range in which the power-law behavior of $n_{\rm cr} \propto T^{\frac{3}{2}}$ is satisfied. At very low temperature, the quadratic approximation to the minimum of the dispersion becomes very accurate. As $T \to 0$, the quadratic dispersion $\epsilon_{\mathbf{k}} = \frac{\mathbf{k}^2}{2m}$ yields $n_{\rm cr} \propto T^{\frac{3}{2}}$ by evaluating Eq.(25) exactly[20] to give

$$\lim_{T\to 0} n_{\rm cr}(T) = \frac{\zeta_{\frac{3}{2}}}{2}\left(\frac{Tm}{2\pi}\right)^{\frac{3}{2}}. \tag{26}$$

In $Ba_3Cr_2O_8$, a low-temperature $T^{\frac{3}{2}}$ fit deviates from the full disperion critical density $n_{\rm cr}$ around 0.06 K as shown in Fig.8. This is an order of magnitude smaller than for $TlCuCl_3$, where the $T^{\frac{3}{2}}$ behaviour persists up to about 0.6 K as described in Fig.9. The lower temperature scale of $Ba_3Cr_2O_8$ is expected to be from the smaller triplon bandwidth, represented by the large effective mass near the dispersion minimum. From the power-law fits to Eq.(26) in Fig.8 and Fig.9 we find that $1/m \cong 1.36$ K (43.6 K) for $Ba_3Cr_2O_8$ ($TlCuCl_3$[21]) showing the narrower bandwidth of $Ba_3Cr_2O_8$. Here we set $\hbar^2/k_B = 1$.

V. SPECIFIC HEAT

We apply the HFP approach to explain the specific heat data measured by M. Kofu *et al.*[13] To determine the magnetic contribution to the specific heat, we first find the expectation value of the energy per dimer. After condensing the triplons at momentum $\mathbf{Q}$, the diagonalized mean-field Hamiltonian contains only number operators of thermally distributed bosonic quasi-

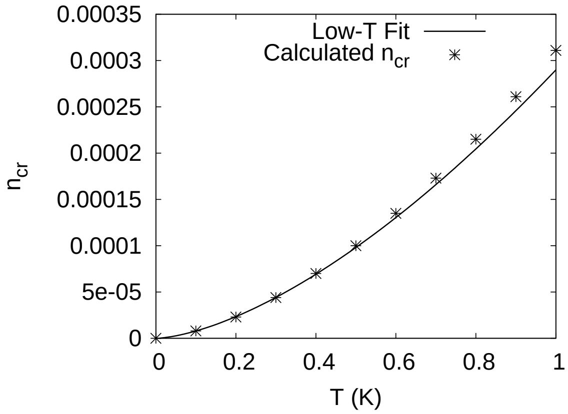

FIG. 9: Same plot as Fig.8 but for the $TlCuCl_3$ compound. Note that the results obtained from the full dispersion follow the power-law fit up to 0.6 K.

particles (see Eqs. (16) and (19)). By differentiating the energy with respect to temperature, we find the specific heat per dimer. In the normal phase,

$$\frac{\langle E\rangle}{N_d} = -Un^2 + \int \frac{\mathrm{d}^3k}{(2\pi)^3}\tilde{\epsilon}_{\mathbf{k}} f_B(\tilde{\epsilon}_{\mathbf{k}}) \tag{27}$$

and

$$\frac{C_V}{N_d k_B} = -\beta \int \frac{\mathrm{d}^3k}{(2\pi)^3}\tilde{\epsilon}^2_{\mathbf{k}} \frac{\partial f_B}{\partial \tilde{\epsilon}_{\mathbf{k}}} + 2U\frac{\partial n}{\partial T}\int \frac{\mathrm{d}^3k}{(2\pi)^3}\tilde{\epsilon}_{\mathbf{k}}\frac{\partial f_B}{\partial \tilde{\epsilon}_{\mathbf{k}}}, \tag{28}$$

with

$$\frac{\partial n}{\partial T} = -\beta \frac{\int \frac{\mathrm{d}^3k}{(2\pi)^3}\tilde{\epsilon}_{\mathbf{k}}\frac{\partial f_B}{\partial \tilde{\epsilon}_{\mathbf{k}}}}{1-2U\int \frac{\mathrm{d}^3k}{(2\pi)^3}\frac{\partial f_b}{\partial \tilde{\epsilon}_{\mathbf{k}}}}. \tag{29}$$

However, in the condensed phase, we have

$$\frac{\langle E\rangle}{N_d} = E_0 - \frac{1}{2}\int \frac{\mathrm{d}^3k}{(2\pi)^3}\tilde{\epsilon}_{\mathbf{k}} + \int \frac{\mathrm{d}^3k}{(2\pi)^3}E_{\mathbf{k}}\left(f_B(E_{\mathbf{k}})+\frac{1}{2}\right) \tag{30}$$

and

$$\frac{C_V}{N_d k_B} = -\beta \int \frac{\mathrm{d}^3k}{(2\pi)^3}E^2_{\mathbf{k}}\frac{\partial f_B}{\partial E_{\mathbf{k}}} + 2U\frac{\partial n}{\partial T}\times \left[n_c - n - \frac{1}{2} + \int \frac{\mathrm{d}^3k}{(2\pi)^3}\frac{\epsilon_{\mathbf{k}}}{E_{\mathbf{k}}}\left(f_B(E_{\mathbf{k}})+\frac{1}{2}+E_{\mathbf{k}}\frac{\partial f_B}{\partial E_{\mathbf{k}}}\right)\right], \tag{31}$$

with

$$\frac{\partial n}{\partial T} = \frac{\beta\int \frac{\mathrm{d}^3k}{(2\pi)^3}\tilde{\epsilon}_{\mathbf{k}}\frac{\partial f_B}{\partial E_{\mathbf{k}}}}{1-2U\int \frac{\mathrm{d}^3k}{(2\pi)^3}\frac{\epsilon_{\mathbf{k}}}{E^2_{\mathbf{k}}}\left(-\tilde{\epsilon}_{\mathbf{k}}\frac{\partial f_B}{\partial E_{\mathbf{k}}}+\frac{\tilde{\mu}}{E_{\mathbf{k}}}(f_B(E_{\mathbf{k}})+\frac{1}{2}\right)}. \tag{32}$$

Non-magnetic contributions to the specific heat, such as phonon contribution, will not change appreciably with the applied field. The difference $C_V(H) - C_V(0)$ thus captures the heat capacity contribution from triplons. Currently, there exists no zero-field specific heat data, preventing proper quantitative comparison.

However, we may still make a comparison, up to an overall scale difference, between the theoretical specific heat and experimental heat capacacity data. Fig.10 shows the calculated magnetic contribution with the experimentally determined heat capacity in Ref.13. The relative scale is chosen to best show similarity in the peak shape for fields close to the zero-temperature critical field. Despite the scale difference and non-triplon contribution, the theoretical result still captures the peak at the critical temperature. However, the drop in heat capacity is overestimated. Furthermore, it is discontinuous, which can be considered as an artifact of the HFP approximation.[21]

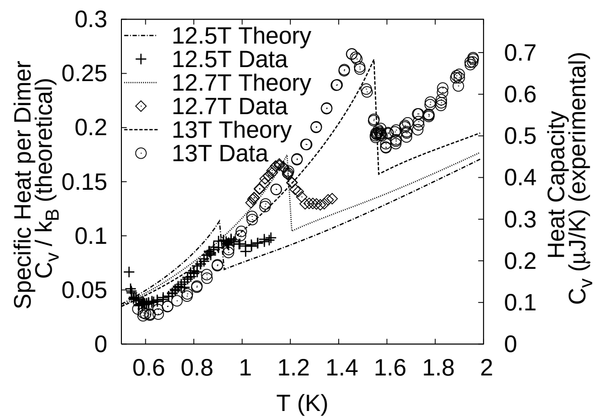

FIG. 10: Comparison of experimental heat capacity to theoretical specific heat per dimer as a function of temperature. Comparisons are made for external fields of 12.5 T, 12.7 T, and 13 T. The experimental data is from Ref.13 with the applied field H parallel to the c-axis.

VI. MAGNETIZATION

When $H > H_c$, γ_+ bosons condense, leading to the macroscopic occupation of the triplet states with the momentum corresponding to the dispersion minimum. The ground state wave function is then given by the coherent superposition of the singlet and the S_z=1 triplet states.[1,18] The density of the condensate determines the magnetization along the z-direction. In addition, the condensate supports the staggered magnetization which has finite transverse components $\langle S_i{}^x\rangle$ and $\langle S_i{}^y\rangle$ breaking the continuous U(1) rotation symmetry around the z direction.

To determine the magnetic ordering, we begin by rewriting the spin operators in terms of the t_0, t_- and t_+ operators. Using the bond operator representation we obtain the following

relations:

$$(S_1+S_2)_\alpha = -i\epsilon_{\alpha\beta\gamma}t^\dagger_\beta t_\gamma,$$
$$(S_1-S_2)_\alpha = s^\dagger t_\alpha + t^\dagger_\alpha s. \tag{33}$$

for $\alpha \in \{x,y,z\}$. Due to Zeeman splitting, the $t_z = \gamma_0$ triplets are negligible, and we find that $\langle (S_1+S_2)_x\rangle = \langle (S_1+S_2)_y\rangle = \langle (S_1-S_2)_z\rangle = 0$. As γ_- are similarly negligible, we expand the rest of the triplet $t_\pm$ operators in terms of the $\gamma_\pm$ operators. After that we ignore the terms with γ_- because they do not contribute to expectation values. The average spin component per dimer along the field direction, which is nothing but the fraction of aligned quasiparticles n, is given by

$$\begin{aligned}\langle(\mathbf{S}_1+\mathbf{S}_2)_z\rangle &= \left\langle t^\dagger_+ t_+ - t^\dagger_- t_-\right\rangle \\ &= \frac{1}{N_d}\sum_{\mathbf{k}}\left\langle \gamma^\dagger_{\mathbf{k}+}\gamma_{\mathbf{k}+}\right\rangle (u^2_{\mathbf{k}-} - v^2_{\mathbf{k}-}) = n.\end{aligned} \tag{34}$$

Since we have condensed singlet $\bar{s}$, the staggered component of the spin becomes (using $u_{-\mathbf{k}} = u_{\mathbf{k}}$)

$$\begin{aligned}\langle S_{i1x} - S_{i2x}\rangle &= \frac{\bar{s}}{\sqrt{2}}\left\langle t^\dagger_{i+} + t^\dagger_{i-} + t_{i+} + t_{i-}\right\rangle \\ &= \frac{\bar{s}}{\sqrt{2N_d}}\sum_{\mathbf{k}} e^{i\mathbf{k}\cdot\mathbf{r}_i}\left\langle t^\dagger_{\mathbf{k}+} + t^\dagger_{\mathbf{k}-}\right\rangle + h.c. \\ &= \frac{\mathrm{sgn}(B)\sqrt{2}\bar{s}}{\sqrt{N_d}}(u_{\mathbf{Q}-} - v_{\mathbf{Q}-})\Re(e^{i\mathbf{Q}\cdot\mathbf{r}_i}\Gamma_{\mathbf{Q}}).\end{aligned} \tag{35}$$

Here $\Gamma_{\mathbf{Q}} = \left\langle \gamma^\dagger_{\mathbf{Q}+}\right\rangle$ with $|\Gamma_{\mathbf{Q}}|^2 = n_c$. Without loss of generality, we fix the overall phase by taking $\Gamma_{\mathbf{Q}}$ to be real. Only the coherent condensate contributes to the transverse magnetization. Similarly, the y-component comes from the imaginary component of the condensate,

$$\langle S_{i1y} - S_{i2y}\rangle = \frac{\mathrm{sgn}(B_{\mathbf{Q}})\sqrt{2}\bar{s}}{\sqrt{N_d}}(u_{\mathbf{Q}-} - v_{\mathbf{Q}-})\Im(e^{i\mathbf{Q}\cdot\mathbf{r}_i}\Gamma_{\mathbf{Q}}). \tag{36}$$

The transverse spin component thus is spatially modulated by the condensate wavevector $\mathbf{Q}$. The transverse magnetization per dimer can be written as[19]

$$M_{xy} \equiv \frac{1}{N_d}\sum_i e^{i\mathbf{Q}\cdot\mathbf{r}_i}\langle S_{i1x} - S_{i2x}\rangle \tag{37}$$
$$\begin{aligned}&= \frac{\mathrm{sgn}(B_{\mathbf{Q}})\sqrt{2}\bar{s}}{\sqrt{N_d}^3}(u_{\mathbf{Q}-} - v_{\mathbf{Q}-})\sum_i e^{i\mathbf{Q}\cdot\mathbf{r}_i}\cos(\mathbf{Q}\cdot\mathbf{r}_i)\Gamma_{\mathbf{Q}} \\ &= \frac{\mathrm{sgn}(B_{\mathbf{Q}})\bar{s}}{\sqrt{2N_d}}(u_{\mathbf{Q}-} - v_{\mathbf{Q}-})\Gamma_{\mathbf{Q}}.\end{aligned} \tag{38}$$

The square of the transverse magnetization per Cr^{5+} ion is then

$$\begin{aligned}M^2_\perp = (g\mu_B M_{xy})^2 &= g^2\mu^2_B\frac{\bar{s}^2\Gamma^2_{\mathbf{Q}}}{8N_d}\frac{(\omega_{\mathbf{Q}} + A_{\mathbf{Q}} - B_{\mathbf{Q}})^2}{2\omega_{\mathbf{Q}}(A_{\mathbf{Q}} + \omega_{\mathbf{Q}})} \\ &= g^2\mu^2_B\frac{\bar{s}^2 n_c}{4}\frac{A_{\mathbf{Q}} - B_{\mathbf{Q}}}{2\omega_{\mathbf{Q}}} = \bar{s}^2 n_c\frac{J_0 g^2}{8\Delta}\mu^2_B.\end{aligned} \tag{39}$$

Having neglected the γ_0 and γ_- triplons, we estimate $\bar{s}^2 \cong 1-n$, using the overall triplet boson constraint. The total and condensed triplet densities, n and n_c, are determined by solving Eq.(22) and Eq.(23) self-consistently.

The transverse magnetization has been measured by the elastic neutron scattering experiments.[13] The applied field is perpendicular to the c-axis. Fig.11 compares theoretical squared perpendicular magnetization at $T = 0.2$ K to the experimental results.[13] Deviation from the experiment occurs most prominently in the critical field. This is caused by discrepancy between the linear fit $H_c \propto n_{\mathrm{cr}}(T)$ and the experimental critical field $H_c(T)$. However, the shape of the magnetization curve past the critical field is properly reproduced. This can be seen in Fig.12, where the theoretical result has been translated to match the experimental critical field. The resulting shape matches over the entire range of fields, with the theoretical magnetization larger by a factor of 1.13. The magnetization also jumps slightly at the critical field. Like the discontinuity in specific heat, this is an artifact of the HFP treatment.[29]

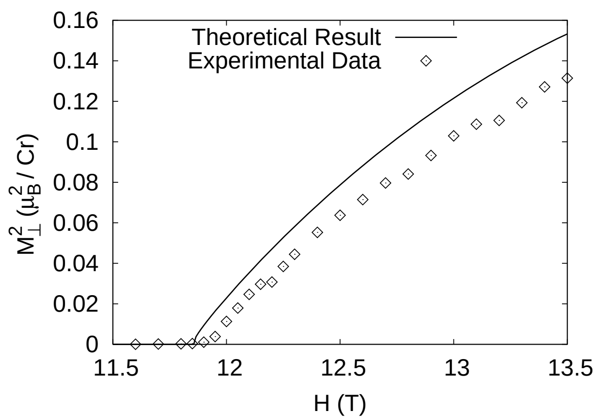

FIG. 11: Comparison of experimental and theoretical perpendicular magnetization squared at $T = 0.2$ K. Perpendicular magnetization is defined in Eq.(37). The experimental data is from Ref.13, with the applied field H perpendicular to the c-axis.

The parallel magnetization has been measured as a function of applied field (both parallel and perpendicular to the c-axis) at the condensate transition.[13] Fig.13 gives the HFP result for H perpendicular to the c-axis, with the magnetization per dimer $M_\parallel = \frac{g}{2}\mu_B n$. The saturation field, where all spins are aligned with the field, is severely underestimated by the HFP result of 18 T. Experimentally it is found between 23 T and 24 T, from the derivative of magnetization $\frac{\partial M}{\partial H}$.[13] This happens because the triplon density in the HFP approach grows too quickly with increasing field.

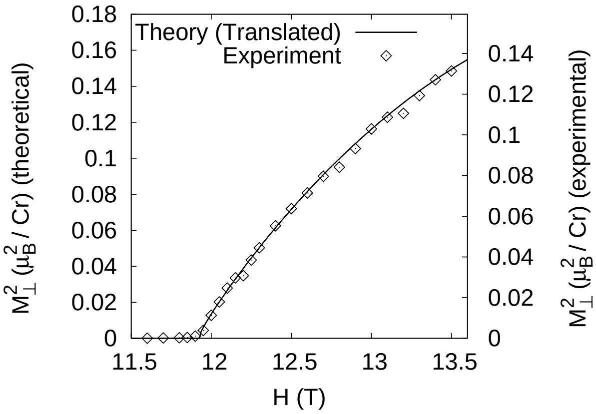

FIG. 12: Comparison of the shape of theoretical and experimental perpendicular magnetization curves as in Fig. 11. Theoretical result has been translated by 0.07 T to match the experimental critical-field behaviour. The scale of the theoretical result is 1.13 larger than that of the experimental data.

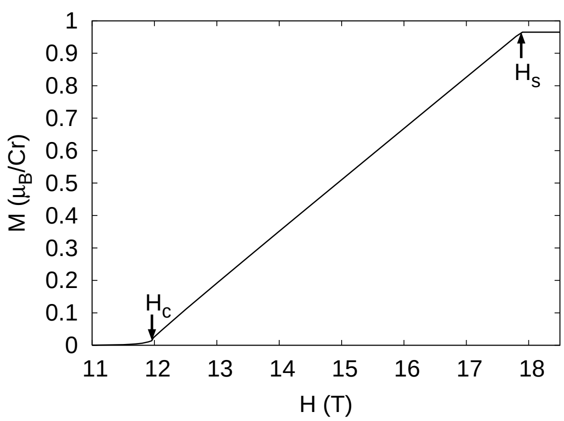

FIG. 13: Parallel magnetization per Cr atom, as a function of applied field perpendicular to the c-axis, at $T = 0.4$ K. The result is found from the triplon density as determined by the HFP approach. Critical field H_c and saturation field H_s are indicated.

VII. DISCUSSION

We have applied the HFP approach to understand the triplon BEC in $Ba_3Cr_2O_8$, using the full dispersion of the triplons measured in the recent neutron scattering experiments (which is recast in the form of a bond-operator representation of a Heisenberg model). We investigated the temperature range where the HFP approach is valid with the full dispersion, and also locates the temperature where the quadratic approximation of the dispersion breaks down. Using this approach, we computed the transverse magnetization and specific heat that are favorably compared to available experimental data. Our results show that the BEC picture overall works reasonably well for $Ba_3Cr_2O_8$.

In the much-studied three-dimensionally-coupled spin-dimer system $TlCuCl_3$, the triplon band width $W \sim 87$ K and the effective interaction $U \sim 340$ K within the HFP analysis.[21] In contrast, our analysis leads to $W \sim 21$ K and $U \sim 8.7$ K in $Ba_3Cr_2O_8$. Thus it may appear that the HFP would work better for $Ba_3Cr_2O_8$ because of smaller U/W. On the other hand, smaller U in $Ba_3Cr_2O_8$ results in a larger critical triplon density $n_{cr} \sim 0.1$ compared to $n_{cr} \sim 0.002$ in $TlCuCl_3$, making the dilute triplon density approximation less valid. In the end, the combined effect in the form of the HFP correction to the critical field $H_c(T)$, Un_{cr}, turns out to be bigger for the case of $Ba_3Cr_2O_8$. This means that the temperature range where the HFP approach is valid is more limited in the case of $Ba_3Cr_2O_8$. Indeed, it is found that the HFP works up to $8K$ in $TlCuCl_3$ while it fits the data up to $2K$ at best in $Ba_3Cr_2O_8$.

The triplon dispersion in $Ba_3Cr_2O_8$ is flatter (or the effective mass is larger) compared to $TlCuCl_3$, which leads to a smaller window of temperatures where the quadratic-dispersion approximation is valid. This is seen in how the relation $[H_c(T) - H_c(0)] \propto T^{3/2}$ reproduces the phase diagram for $T < 0.1$ K for $Ba_3Cr_2O_8$, but for $T < 1$ K in $TlCuCl_3$.

A useful way to improve the HFP results may be to introduce the hard-core constraint among the triplons. The so-called Bruckner bond operator approach[26,27] achieves this by introducing an infinite on-site triplon repulsion by

$$\mathcal{H}_C = V \sum_{i\alpha\beta} t^\dagger_{i\alpha} t^\dagger_{i\beta} t_{i\alpha} t_{i\beta} \tag{40}$$

as $V \to \infty$. In the low-density limit, this hard-core interaction may be treated exactly by a summation of ladder diagrams at the one-loop level in the self-energy. This approach, when generalized to finite temperature, should lower the triplon densities and extend the region where low-density approximations are valid. This may be a useful future extension of our work.

Recent ESR measurements indicate the existence of siglet-triplet mixing in the ground state of $Ba_3Cr_2O_8$.[13] In the ground state, singlets mix with t_0 for $H \perp c$, and with $t_\pm$ for $H \parallel c$. This mixing points to the existence of a Dzyaloshinsky-Moriya (DM) interaction of the form $\mathbf{D}_{ij} \cdot \mathbf{S}_i \times \mathbf{S}_j$, with $\mathbf{D}_{ij}$ perpendicular to the c-axis. Since it breaks the U(1) symmetry of the Heisenberg Hamiltonian, the system is no longer described by a BEC transition. The result is that triplons are gapped and always condensed to some extent, turning the transition into a crossover region.[28,29] Below the temperature scale of the DM interaction, then, we expect that a simple BEC picture of triplons will no longer be sufficient. This could explain, for instance, the nonlinearity of critical field H_c in critical density $n_{\rm cr}$ at low temperatures for H perpendicular to the c-axis. An understanding of the magnitude and direction of the $\mathbf{D}_{ij}$ vector is important for a proper and full description of $Ba_3Cr_2O_8$, especially at very low temperatures.

Acknowledgments

We thank S. H. Lee for providing the experimental data on $Ba_3Cr_2O_8$ and many helpful discussions. This work was sup-

ported by the NSERC of Canada, the Canada Research Chair program, and the Canadian Institute for Advanced Research. We also acknowledge the hospitality of the Kavli Institute for Theoretical Physics and the Aspen Center for Physics, where various parts of this work were performed.

[1] T. Giamarchi, Ch. Rüegg, and O. Tchernyshyov, Nature Phys. **4**, 198 (2008).
[2] T. M. Rice, Science **298**, 760 (2002).
[3] K. Kodama, M. Takigawa, M. Horvati, C. Berthier, H. Kageyama, Y. Ueda, S. Miyahara, F. Becca, and F. Mila, Science **298**, 395 (2002).
[4] H. Kageyama, K. Yoshimura, R. Stern, N. V. Mushnikov, K. Onizuka, M. Kato, K. Kosuge, C. P. Slichter, T. Goto, and Y. Ueda, Phys. Rev. Lett. **82**, 3168 (1999).
[5] A. Oosawa, M. Ishii, and T. Tanaka, J. Phys. Condens. Matter **11**, 265 (1999).
[6] Ch. Rüegg, N. Cavadini, A. Furrer, H.-U. Güdel, K. Krämer, H. Mutka, A. Wildes, K. Habicht and P. Vorderwisch, Nature **423**, 62 (2003).
[7] M. Jaime, V. F. Correa, N. Harrison, C. D. Batista, N. Kawashima, Y. Kazuma, G. A. Jorge, R. Stern, I. Heinmaa, S. A. Zvyagin, Y. Sasago, and K. Uchinokura, Phys. Rev. Lett. **93**, 087203 (2004).
[8] S.E. Sebastian, N. Harrison, C. D. Batista, L. Balicas, M. Jaime, P. A. Sharma, N. Kawashima, and I. R. Fisher, Nature **416**, 617 (2006).
[9] Ch. Ruegg, D. F. McMorrow, B. Normand, H. M. Rłnnow, S. E. Sebastian, I. R. Fisher, C. D. Batista, S. N. Gvasaliya, Ch. Niedermayer, and J. Stahn Phys. Rev. Lett. **98**, 017202 (2007).
[10] S. Kramer, R. Stern, M. Horvatic, C. Berthier, T. Kimura, and I. R. Fisher Phys. Rev. B. **76**, 100406(R) (2007).
[11] N. Laflorencie and F. Mila Phys. Rev. Lett. **102**, 060602 (2009).
[12] M. Kofu, J.-H. Kim, S. Ji, S.-H. Lee, H. Ueda, Y. Qui, H.-J. Kang, M. Green, and Y. Ueda, Phys. Rev. Lett. **102**, 037206 (2009).
[13] M. Kofu, H. Ueda, H. Nojiri, Y. Oshima, T. Zenmoto, K.C. Rule, S. Gerischer, B. Lake, C.D. Batista, Y. Ueda, and S.-H. Lee, Phys. Rev. Lett. **102**, 177204 (2009).
[14] T. Nakajima, H. Mitamura, and Y. Ueda, J. Phys. Soc. Jpn. **75**, 054706 (2006).
[15] Y. Singh and D. C. Johnston, Phys. Rev. B **76**, 012407 (2007).
[16] A. A. Aczel, Y. Kohama, M. Jaime, K. Ninios, H.B. Chan, L. Balicas, H.A. Dabkowska, and G.M. Luke, Phys. Rev. B. **79**, 100409 (2009).
[17] H. Tsujii, B. Andraka, M. Uchida, H. Tanaka, and Y. Takano Phys. Rev. B **72**, 214434 (2005).
[18] M. Matsumoto, B. Normand, T. M. Ride, and M. Sigrist, Phys. Rev. Lett **89**, 077203 (2002).
[19] M. Matsumoto, B. Normand, T. Ride, and M. Sigrist, Phys. Rev. B **69**, 054423 (2004).
[20] T. Nikuni, M. Oshikawa, A. Oosawa, and H. Tanaka, Phys. Rev. Lett. **84**, 5868 (2000).
[21] G. Misguich and M. Oshikawa, J. Phys. Soc. Jpn. **73**, 3429 (2004).
[22] F. Yamada, T. Ono, H. Tanaka, G. Misguich, M. Oshikawa, and T. Sakakibara, J. Phys. Soc. Jpn. **77**, 3701 (2008).
[23] A. V. Chubukov, JETP Lett. **50**, 129 (1989).
[24] S. Sachdev and R. Bhatt, Phys. Rev. B. **41**, 9323 (1990).
[25] J.P. Blaizot and G. Ripka, "Quantum theory of finite systems" (MIT Press, Massachusetts, 1986).
[26] O. Rosch and Matthias Vojta, Phys. Rev. B **76**, 224408 (2007).
[27] V.N. Kotov, O. Sushkov, Zheng Weihong, and J. Oitmaa, Phys. Rev. Lett. **80**, 5790 (1998).
[28] J. Sirker, A. Weisse, and O. Sushkov, Europhys. Lett. **68**, 275 (2004).
[29] J. Sirker, A. Weisse, and O. Sushkov, J. Phys. Soc. Jpn. Supp. **74**, 129 (2005).